Hindawi
International Journal of Analytical Chemistry
Volume 2022, Article ID 6805501, 6 pages
https://doi.org/10.1155/2022/6805501

Research Article

Influence of Nanosemiconductor Materials on Thermal Stability of Solar Cells

Aijie Ma

Hebei Chemical & Pharmaceutical College, Shijiazhuang 050026, China

Correspondence should be addressed to Aijie Ma; 201704404@stu.ncwu.edu.cn

Received 30 May 2022; Revised 9 June 2022; Accepted 20 June 2022; Published 4 July 2022

Academic Editor: Nagamalai Vasimalai

In order to overcome the problem of long-term stability of perovskite solar cells, the author proposes a method to study the effects of nanosemiconductor materials on the thermal stability of solar cells. In this method, $n=3$ and $n=1$ $(C_6H_5(CH_2)_2NH_3)_2(CH_3NH_3)_{n-1}Pbn\ I_{3n+1}$ two-dimensional nanoperovskite films were investigated on glass substrates and indium tin oxide (ITO) substrates, respectively, on the thermal stability. Experimental results show that the glass-based nanoperovskite $PMPI_3$ film was partially decomposed into PbI_2 after being heated at 160°C. When the temperature reaches 180°C, the film is completely decomposed into PbI_2, and the perovskite $PMPI_3$ film with ITO as the substrate is completely decomposed into PbI_2 when the heating temperature reaches 140°C. The charge transfer between the perovskite film and the substrate is the physical reason for its easier thermal decomposition on the ITO substrate. Suggestions for improving the thermal stability of perovskite solar cell devices are given from the aspects of device design and fabrication process.

1. Introduction

Perovskite solar cells (PSCs) have become a research hotspot in the field of efficient utilization of solar energy due to their excellent optoelectronic properties. After more than ten years of optimization of perovskite materials and improvement of cell structure, the photoelectric conversion efficiency of single-junction PSCs has increased from 3.8% in 2009 to 25.5% certified in 2020 and is expected to become the first choice for a new generation of thin-film solar cells [1]. At present, the vast majority of PSCs use the TiO_2 mesoporous structure as the electron transport layer. However, the perovskite material has a low pore filling rate in the mesoporous structure and a large photogenerated charge transfer resistance, which is the main reason to limit the further improvement of the performance of this type of PSCs.

At present, perovskite solar cells mainly have two basic structures: mesoscopic and planar structures. Compared with the planar structure, the PSCs of the mesoscopic structure are mainly composed of five parts: transparent electrode, electron transport layer, perovskite light absorption layer, hole transport layer, and back electrode. According to the structure of the electron transport layer, the mesoscopic structure is further divided into the mesoporous structure and the nanoarray structure. Nanoparticles in the mesoporous structure can increase light scattering, improve the solar light capture efficiency of the battery, and at the same time, has a large specific surface area, which can increase the contact area between the perovskite and the electron transport layer. This in turn improves battery efficiency. Single-crystal TiO_2 nanorod arrays (titanium dioxide nanorod arrays, TNRAs) have unobstructed electron transport channels and through-ordered pore structure, and the one-dimensional single-crystal nanorods have fewer grain boundaries and defects. At the same time, the orderly and through pores are easy to be filled with perovskite materials, which increases the contact area between TNRAs and perovskite, which can effectively make up for the lack of TiO_2 mesoporous structure. This has attracted the attention of many researchers [2]. However, the perovskite layers deposited on TNRAs suffer from low coverage and high defect density, and the "TNRAs/perovskite" interfacial contact is problematic. As a result, the photoelectric

conversion efficiency and stability of TNRAs-based PSCs are still not ideal [3]. How to optimize the contact and energy level matching between the "TNRAs/perovskite" interface, passivate the defects of perovskite films, and further improve the performance of TNRAs-based PSCs has become an urgent problem to be solved as shown in Figure 1.

2. Literature Review

Yu et al. fabricated α-$CsPbI_3$ QD films that were stable in air for several months and reduced the size of the crystallites to nanoscale by preparing them into quantum dots. Thus, the phase stabilization temperature of α-$CsPbI_3$ is well controlled. The perovskite QD photovoltaic cells were fabricated, the open circuit voltage is 1.23 V, and the efficiency is 10.77%. The efficiency did not decrease after aging for 1440 h in air, demonstrating the humidity stabilization potential of $CsPbI_3$ [4]. Xin et al. used graphene oxide to cross-link quantum dots to form graphene/$CsPbI_3$ films, and the graphene cross-linking restricted the position of quantum dots in order to ensure that the high surface energy characteristics of quantum dots can be exerted. The graphene layer plays a blocking role against water within the device structure, and at the same time, the higher mobility ensures the transmission of excitons. When the device was placed at 60% humidity for 5 h, the efficiency decreased by only 10% of the initial level, showing good stability [5]. Hu et al. designed a gradient particle size (GGS) $CsPbI_3$ bilayer. Let ADMA interact with perovskite, and a large-grained $CsPbI_3$ layer was obtained at the bottom position with high charge mobility and low density of well states. This gradient particle size not only ensures higher surface energy of the upper layer material but also ensures that the lower layer material has fewer grain boundary defects. The device operates stably for 1 000 h at room temperature and a relative humidity of 20%, with an efficiency retention of 85% [6]. Selvanathan et al. developed the spontaneous interface modification (SIM) technique, which can spontaneously organize the 2D/3D perovskite top interface without the use of weakly polar solvents, resulting in a 2D/3D multidimensional perovskite top layer. The spontaneously formed ultrathin 2D perovskite not only eliminates interfacial defects but also effectively hinders moisture permeation. Finally, the CsPbIxBr3-x all-inorganic device obtained a significant efficiency improvement, the photoelectric conversion efficiency increased from 13, from 64% to 18%, and the device life is also greatly extended. The device can still retain 81% of the efficiency when stored in air for 1000 h [7]. Dong et al. found that, compared with the traditional MDMO-PPV system, P3HT has better crystallinity, and P3HT can form longer nanowhiskers under thermal annealing conditions. On the one hand, these nanowhiskers can improve the hole mobility of the photoactive layer, and on the other hand, it has a certain inhibitory effect on the migration and aggregation of PC61BM. This finding has a positive effect on the later study of using P3HT nanowhiskers to improve the thermal stability of the device [8].

Therefore, in order to further study the thermal stability of nanoperovskite materials, for improving the stability of perovskite and promoting perovskite solar cells, the application in people's life is of great significance. The authors prepared $(PEA)_2(CH_3NH_3)_{n-1}[Pb_n\ I3_{n+1}]n = 1$ and 3 films on glass and indium tin oxide (ITO) substrates, respectively, PEA = $C_6H_5(CH_2)_2NH_3$. The thermal stability of $PEA_2MA_2Pb_3I_{10}(PMPI_3)$ films and $PEA2PbI_4$(PEPI) films on two substrates at different temperatures were systematically studied, MA = CH_3NH_3.

3. Research Methods

In the experiment, the glass substrate and ITO substrate (15 Ω/sq) were first put into deionized water for 15 min and then placed in anhydrous alcohol for 15 min; finally, the cleaned substrate was blow-dried with high-purity nitrogen and treated with ultraviolet ozone for 30 min to enhance the wettability of the substrate surface. The dimensions of the glass substrate and the ITO substrate are both 1.5 cm × 1.5 cm. PEAI (124.5 mg), MAI (79.5 mg), and PbI2 (345.75 mg) in a molar ratio of 2 : 2:3 were dissolved in 875 mL of DMF solvent and stirred for 5 h on a heating table at 45°C to obtain nanoperovskite PMPI3 precursor solution [9]. 400 mg of PEPI was dissolved in 635 mL of DMF solvent and stirred on a heating table at 45°C for 5 h to obtain the nanoperovskite PEPI precursor solution. PbI_2 and MAI were purchased from Xi'an Baolite Company, and DMF was purchased from Alfa Aesar Company. Two perovskite precursor solutions were spin-coated onto the treated glass and ITO substrates, respectively, the speed of the spin coater was 4000 r/s, and the time was 30 s. Then, the PMPI3 perovskite films on the glass substrate and the ITO substrate were heated at 100°C, 120°C, 140°C, 160°C, 180°C, and 200°C for 15 min on a heating stage, respectively, the PEPI perovskite films on glass substrates and ITO substrates were heated at 100°C, 120°C, 140°C, 160°C, 180°C, and 200°C for 15 min, respectively. The above experimental operations were completed in a nitrogen-filled glove box [10].

After the preparation of the samples, the absorption of these annealed films was measured, and X-ray diffraction (XRD) and photoluminescence were used to characterize the decomposition degree of perovskite in the films and the decomposition products. The absorption spectra of the perovskite films were measured with an EVOLUTION220 UV-Vis spectrophotometer, the XRD patterns were measured by a Bruker AXS DimensionD8 X-ray system, and the photoluminescence spectra were measured by an optical system built in the laboratory and excited by a laser with a wavelength of 447 nm [11].

In the process of evaluating whether the perovskite lattice is stable, we usually use the tolerance factor as the criterion for judgment. The ionic radius matching in the perovskite structure should satisfy the following formula:

$$R_A + R_X = \sqrt{2}(R_B + R_X) \cdot t, \tag{1}$$

where R_A, R_B, and R_X represent the ionic radii of A, B, and X, respectively, $t = 1$ is an ideal octahedron with a common vertex connection structure.

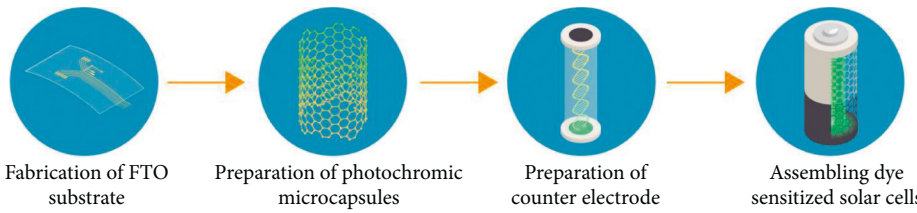

Figure 1: Flow chart of thermal stabilization of solar cells.

4. Analysis of Results

As shown in Figures 2(a) and 2(b), nanoperovskite $PMPI_3$ thin films based on ordinary glass and ITO conductive glass, respectively, were heated at 100°C, 120°C, 140°C, 160°C, 180°C, and 200°C for 15 min after the absorption spectrum. The absorption spectrum shows that $PMPI_3$ film has three absorption peaks at 601 nm, 566 nm, and 515 nm, respectively. The absorption peak at 602 nm is generated by the absorption of $n = 3$ materials, the absorption peaks at 515 nm and 566 nm correspond to the exciton absorption energies of $n = 1$ and $n = 2$ materials, respectively, and at the same time, there is obvious absorption below 602 nm. This is because the PEA_2 $(MA)_{n-1}$ Pb_n $I3_{n+1}$ nanoperovskite with larger n value exists in the film. It can be seen that although the molar ratio of $n = 3$ is used to configure the solution during the preparation of $PMPI_3$ films, and the films prepared by spin coating are mixed films containing nanoperovskites with various n values [12]. From Figure 2(a), it can be found that, after annealing at 100°C, 120°C, and 140°C, the absorption spectra of the films basically overlap without obvious changes. At the same time, when the heating temperature increases to 160°C in Figure 2(a), the three absorption peaks of perovskite still exist, but the intensity becomes weaker. These phenomena indicate that the film at this temperature has partially decomposed. When the heating temperature was increased to 180°C and 200°C, the absorption peaks at 515 nm, 602 nm and 566 nm of the film disappeared, but appeared as a rapidly changing absorption band edge at 520 nm, and the color of the film changed completely to yellow [13]. It can be seen from Figure 2(b) that when the heating temperature is 100°C and 120°C, the three absorption peaks of the perovskite are clearly displayed. When the heating temperature rises to 140°C, the decomposition of the $PMPI_3$ film on the ITO substrate has been completed, and the film turns yellow completely. When the heating temperature is 160–200°C, and the absorption spectrum and the color of the film on the ITO substrate are completely consistent with those at 140°C. These phenomena indicate that the ITO-based perovskite $PMPI_3$ material is completely decomposed after heating at 140°C. Combined with the above experimental results, it is found that the nanoperovskite PMPI3 film with ITO as the substrate, and it is more prone to thermal decomposition than thin films on glass substrates [14].

In order to understand the process and products of thermal decomposition, the XRD of each film studied in Figure 2 was measured, and the distribution of PbI_2 and nanoperovskite $PMPI_3$ in the heat-treated films was further studied. Figures 3(a) and 2(b) show the nanoperovskite $PMPI_3$ with ordinary glass and ITO conductive glass as substrates at 100°C, 120°C, 140°C, 160°C, 180°C, and 200°C, respectively, on the heating stage XRD patterns after heating for 15 min. From Figure 3(a), it is found that the films have consistent and highly similar diffraction peaks when the heating temperature is 100°C, 120°C, and 140°C, and the diffraction peaks (111) and (222) are characteristic peaks of nanoperovskite $PMPI_3$. At the same time, the XRD pattern only shows the characteristic peaks of the nanoperovskite $PEA_2MA_{n-1}Pb_n$ $I3_{n+1}$ with $n = 3$. Although the characteristic peaks of $n = 1$ and $n = 2$ materials are clearly reflected in the absorption spectrum. However, it does not appear in the XRD pattern, indicating that the crystal structure of the nanoperovskite film is still determined by the material of $n = 3$, and other perovskites with different n values exist in the film as "impurity grains." When the temperature was increased to 160°C, the XRD pattern showed that, in addition to the diffraction peaks specific to the nanoperovskite $PMPI_3$, the diffraction peak of PbI_2 appears at $2\theta = 12.7°$, and the intensity of the diffraction peak of perovskite becomes weaker. When the heating temperature is 180°C and 200°C, except for the diffraction peak of PbI_2, the film has no characteristic peaks of perovskite materials [15]. It can be seen from Figure 3(b) that when the heating temperature is 100°C and 120°C, the PMPI3 film on the ITO substrate has similar nanoperovskite $PMPI_3$ diffraction peaks, and the film only has the diffraction peak of PbI_2 at 140–200°C. In summary, it is found that the nanoperovskite $PMPI_3$ film on glass substrate is partially decomposed into PbI_2 after heating at 160°C, and when the temperature reaches 180°C, the film is completely decomposed into PbI_2, and the perovskite $PMPI_3$ film on ITO substrate is completely decomposed into PbI_2 when the heating temperature reaches 140°C.

In the absorption spectrum of Figure 2 and the XRD pattern of Figure 3, the thermal stability of the perovskite $PMPI_3$ film on the ITO substrate is worse. The reason for this phenomenon may be the same as that of the three-dimensional perovskite $MAPbI_3$, it is the charge transfer between the film and the substrate, regardless of whether the perovskite loses or gains electrons, resulting in the decomposition reaction.

In order to further verify the effect of charge transfer, the above experiments were repeated with $n = 1$ nanoperovskite PEPI. The exciton binding energy in PEPI films is as high as ~230 meV, and the quality of the films prepared from solution is relatively high; substantially, no carriers are generated in the case of photoexcitation; therefore, the general

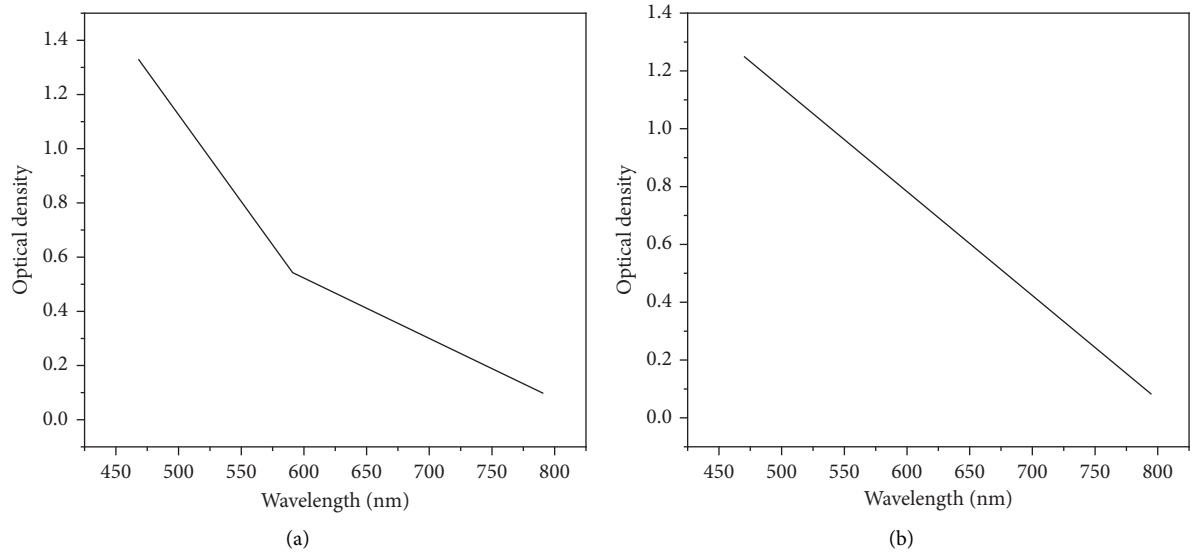

Figure 2: Absorption spectra of $PMPI_3$ films treated at different temperatures. (a) $PMPI_3$/glass. (b) $PMPI_3$/ITO.

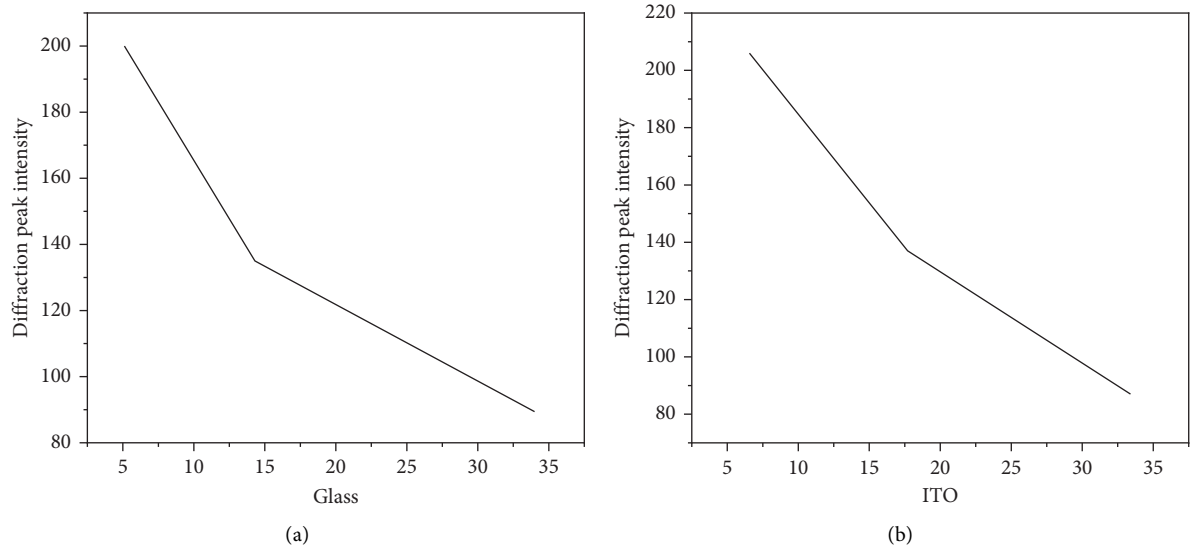

Figure 3: XRD patterns of PMPI3 films treated at different temperatures. (a) $PMPI_3$/glass. (b) $PMPI_3$/ITO.

film does not contain free or bound charges [16]. So, even if the substrate is ITO, there is very little chance of charge transfer between the film and the substrate. It was found that different substrates had little effect on the thermal stability of PEPI films. When the annealing temperature is 160°C, the films have very clear X-ray diffraction structures belonging to PEPI films. This also shows that the PEPI film has high crystallinity and good quality. After annealing at 180°C and 200°C, the X-ray diffraction peaks have basically presented the PbI_2 film structure. But comparing the absorption spectra, although the spectra of the films annealed at 180°C and those annealed at 160°C are different, there are still obvious PEPI exciton absorption peaks. The film annealed at 180°C lacks the X-ray diffraction structure, indicating that the nanocrystalline structure of the film has been destroyed, but the nm-scale PEPI grains may still exist [17].

In order to further understand the effect of high temperature annealing on perovskite films, the photoluminescence spectra of PEPI films on glass substrates and PEPI films on ITO substrates were further measured. Figure 4 shows the normalized luminescence spectrum of the thin film heated at 100–200°C [18]. Although the luminescence peak of the film annealed at 180°C is slightly broadened compared to other temperatures, it is basically at the same position, which is the luminescence spectrum of PEPI, which is consistent with the absorption spectrum. It was also proved that when the PEPI film was annealed at 180°C, although the X-ray diffraction spectrum showed that the nanocrystalline structure had been destroyed, it still had the coexistence of PbI_2 and PEPI. Under the same experimental conditions, the film annealed at 200°C did not find obvious light-emitting structure, which may be due to the

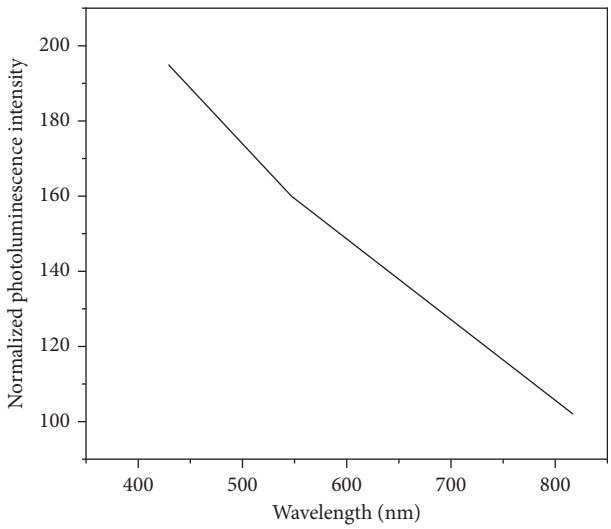

Figure 4: PL spectrum.

fact that although the PbI_2 film itself can also be used as a light-emitting material, the luminous efficiency at room temperature is low, and the experimental system is not sensitive enough.

For the integrity of the experiment, the photoluminescence spectra of $PMPI_3$ films on glass substrates ($PMPI_3$/glass) and $PMPI_3$ films on ITO substrates ($PMPI_3$/ITO) after different temperature treatments were measured. The material annealed at 180°C and 200°C has no obvious light-emitting structure. The luminescence peaks of $PMPI_3$/glass films are all at 780 nm, and the energy is lower than the exciton peak of $n = 3$ (602 nm) because the wavelength of the laser is 447 nm, which should be affected by the nanoperovskites with different n values in the film. The luminescence peak position is close to the component of $n = \infty$, that is, the luminescence peak position of $MAPbI_3$, indicating that there is high-efficiency energy transfer in the film until complete decomposition. However, the $PMPI_3$/ITO films show very different results. First, the luminescent structures of the films at 100°C and 120°C are basically the same as those of $PMPI_3$/glass, the film at 120°C has a more obvious red shift, but it is basically around 750 nm. The luminescence peaks at 140°C and 160°C occurred at 520 nm, which were obviously consistent with the luminescence peaks of PEPI. The charge transfer with the ITO substrate led to the dissociation of the $PMPI_3$ (which should also include the $n = 2$ phase) film that is prone to charge generation, but part of the PEPI grains survived, which dominated the luminescence of the film after annealing at 140°C and 160°C process [19]. At higher temperatures, PEPI also eventually dissociates to PbI_2.

The charge transfer between the perovskite layer and the ITO substrate results in excess holes or electrons in the film. When excess holes appear in the perovskite film, I^- will form I with the excess holes, $(CH_3NH_3Pb)^{3+}$ will react with I to generate CH_3NH_2, HI, PbI_2, and holes, CH_3NH_2 and HI will volatilize as gas, and the generated holes will continue to interact with I^- to promote the reaction. When excess electrons appear in the perovskite, $(CH_3NH_3Pb)^{3+}$ gets electrons to generate CH_3NH_2 and H, H and PbI^{-3} form HI, PbI_2 and electrons, CH_3NH_2 and HI volatilize in the form of gas, the generated electrons will continue, and the role of $(CH_3NH_3Pb)^{3+}$ promotes the reaction [20]. Therefore, when fabricating devices based on nanoperovskite materials, the influence of electrodes needs to be considered during the annealing process of the devices, or a barrier layer of suitable thickness should be inserted between the active layer and the electrodes, for example, Sb_2S_3, it is possible to improve the thermal stability of the device without affecting the photocurrent [21].

5. Conclusion

The stability of nanoperovskite $PMPI_3$ thin films with ordinary glass and ITO conductive glass as substrates at different temperatures was investigated, the experimental results show that $PMPI_3$ film on glass substrate is partially decomposed into PbI_2 after heating at about 160°C for 15 min, at the heating temperature of 180°C and higher, the film is basically completely decomposed into PbI_2, and the film on the ITO substrate begins to partially decompose into PbI_2 in the temperature range of 120–140°C. When the temperature was raised to 140°C, the perovskite film was completely decomposed into PbI_2. Therefore, it can be considered that the thermal stability of nanoperovskite $PMPI_3$ on ordinary glass substrate is significantly better than that of perovskite on ITO substrate. For the integrity of the experiment, the thermal stability experiments of nanoperovskite PEPI films on two substrates were performed. By comparing the experimental results, it is found that the thermal stability of the nanoperovskite $PMPI_3$ film based on ITO is worse than that of the film on the glass substrate, and the thermal stability of the nanoperovskite PEPI film on the two substrates is different. Combining the two experimental results, it is believed that the charge transfer between the perovskite material and the substrate may lead to the deterioration of the thermal stability of the perovskite film.

Data Availability

The data used to support the findings of this study are available from the corresponding author upon request.

Conflicts of Interest

The author declares no conflicts of interest.

References

[1] K. Sharma and B. K. Chaurasia, "Trust based location finding mechanism in VANET using DST," in *Proceedings of the Fifth International Conference on Communication Systems & Network Technologies*, pp. 763–766, IEEE, Gwalior, India, April 2015.

[2] R. Grisorio, E. Fanizza, I. Allegretta et al., "Insights into the role of the lead/surfactant ratio in the formation and passivation of cesium lead bromide perovskite nanocrystals," *Nanoscale*, vol. 12, no. 2, pp. 623–637, 2020.

[3] H. Saoudi, A. Benali, M. Bejar et al., "Morphological and electrical properties of la0.8ca0.1pb0.1feo3 perovskite

nanopowder for nh3 and co gas detection," *Journal of Electroceramics*, vol. 45, no. 2, pp. 39–46, 2020.

[4] W. Yu, X. Sun, M. Xiao et al., "Recent advances on interface engineering of perovskite solar cells," *Nano Research*, vol. 15, no. 1, pp. 85–103, 2022.

[5] W. Xin, W. Pengfei, Z. Haiyan et al., "Ultra-broadband near-infrared photoluminescence in er3+-ni2+co-doped transparent glass ceramics containing nano-perovskite kznf3 - sciencedirect," *Ceramics International*, vol. 46, no. 16, pp. 25987–25991, 2020.

[6] Y. H. Hu, M. J. Li, Y. P. Zhou, H. Xi, and T. C. Hung, "Multi-physics investigation of a gaas solar cell based pv-te hybrid system with a nanostructured front surface," *Solar Energy*, vol. 224, no. 3, pp. 102–111, 2021.

[7] V. Selvanathan, R. Yahya, M. Shahiduzzaman et al., "Ionic liquid infused starch-cellulose derivative based quasi-solid dye-sensitized solar cell: exploiting the rheological properties of natural polymers," *Cellulose*, vol. 28, no. 9, pp. 5545–5557, 2021.

[8] S. Dong, L. Sun, and F. Yue, "Influence of selenium growth condition on the photovoltaic conversion efficiency of sb2se3 as the solar cell absorption layer," *Journal of Materials Science: Materials in Electronics*, vol. 33, no. 13, pp. 10335–10342, 2022.

[9] M. Bradha, N. Balakrishnan, S. Suvi et al., "Experimental, computational analysis of butein and lanceoletin for natural dye-sensitized solar cells and stabilizing efficiency by iot," *Environment, Development and Sustainability*, vol. 24, 2022.

[10] A. C. Celline, A. Y. Subagja, S. Suryaningsih, A. Aprilia, and L. Safriani, "Synthesis of tio2-rgo nanocomposite and its application as photoanode of dye-sensitized solar cell (dssc)," *Materials Science Forum*, vol. 1028, pp. 151–156, 2021.

[11] X. Liu, C. Ma, and C. Yang, "Power station flue gas desulfurization system based on automatic online monitoring platform," *Journal of Digital Information Management*, vol. 13, no. 6, pp. 480–488, 2015.

[12] C. Dong, Y. Meng, B. Wang, W. Zhu, and Z. Pang, "Effect of antisolvents on the structure of regenerated cellulose: development of an efficient regeneration process," *Holzforschung*, vol. 74, no. 9, pp. 881–890, 2020.

[13] R. Huang, "Framework for a smart adult education environment," *World Transactions on Engineering and Technology Education*, vol. 13, no. 4, pp. 637–641, 2015.

[14] D. Yang, Z. Fang, Y. Zheng et al., "Pink-emitting rbbabp2o8: sm phosphor with diamondoid structure and high thermostability," *Ceramics International*, vol. 47, no. 15, pp. 21828–21836, 2021.

[15] M. Gurturk, H. Benli, and N. K. Erturk, "Determination of the effects of temperature changes on solar glass used in photovoltaic modules," *Renewable Energy*, vol. 145, pp. 711–724, 2020.

[16] H. Latif, R. Zahid, S. Rasheed et al., "Effect of annealing temperature of moo3 layer in moo3/au/moo3 (mam) coated pbs qds sensitized zno nanorods/fto glass solar cell," *Solar Energy*, vol. 198, pp. 529–534, 2020.

[17] J. Gu, W. Wang, R. Yin, C. V. Truong, C. V. Truong, and B. P. Ganthia, "Complex circuit simulation and nonlinear characteristics analysis of GaN power switching device," *Nonlinear Engineering*, vol. 10, no. 1, pp. 555–562, 2021.

[18] T. Azizi, Z. Kaddachi, M. B. Karoui, A. E. Touihri, and R. Gharbi, "Electrical characterization and efficiency enhancement of dye sensitized solar cell using natural sensitizer and tio_2 nanoparticles deposited by electrophoretic technique," *IEEE Journal of Photovoltaics*, vol. 5, pp. 1–10, 2021.

[19] T. Gunji, K. Nakamura, R. Hayami, A. Aimi, K. Fujimoto, and K. Yamamoto, "Synthesis of indium tin oxide films from ethyl acetoacetonato complexes at low temperatures," *Journal of Sol-Gel Science and Technology*, vol. 100, no. 1, pp. 68–73, 2021.

[20] A. M. Bagov, A. I. Khasanov, and M. Zubkhadzhiev, "Influence of doping with indium onto contact melting of tin and bismuth," *Materials Science Forum*, vol. 1022, pp. 174–180, 2021.

[21] C. Ruan, Q. Sun, D. Xiao, H. Li, G. Xia, and S. Wang, "Lightwave irradiation-assisted low-temperature solution synthesis of indium-tin-oxide transparent conductive films," *Ceramics International*, vol. 48, no. 9, pp. 12317–12323, 2022.